Energetic Probing for the Electron Transfer Reactions Sensitized by 9,10-Dicyanoanthracene and 9-Cyanoanthracene and Their Modified Zeolite Particles

Yu Chen Chang, Pei Wen Chang, and Chong Mou Wang*

Department of Chemistry, National Taiwan Normal University, Taipei 116, Taiwan

Received: August 9, 2002; In Final Form: November 22, 2002

The photooxidation of diphenylamine (DPA) and triphenylphosphine ($P(C_6H_5)_3$) sensitized by 9,10-dicyanoanthracene (DCA) and 9-cyanoanthracene (CA) was investigated in this work. Theoretically and evidently, DPA could quench the excited DCA and CA (denoted DCA* and CA*) via an electron transfer pathway. The Stern−Volmer quenching rate constants were calculated to be ca. 4×10^4 equiv^{-1} s^{-1} for both DCA* and CA*. In contrast to DPA, $P(C_6H_5)_3$ showed no quenching effects on DCA* and CA* and only $P(C_6H_5)_3$ was excited along with the sensitizers upon the exposure to UV light (260 nm). The formal potentials of $DCA^{*/-}$ and $CA^{*/-}$ were thus concluded to be located between the formal potentials of $DPA^{+/0}$ (1.5 V vs SCE) and the formal potentials of $P(C_6H_5)_3{}^{+/0}$ (ca. 2 V vs SCE). Oxygen could significantly quench DCA* and CA* via an energy transfer pathway. Photooxygenations of $P(C_6H_5)_3$ and $(C_6H_5)_3CH$ were carried out using the DCA- and CA-exchanged zeolite particles (denoted NaY/DCA and NaY/CA) as the heterogeneous catalysts. Noticeably, as DCA and CA were adsorbed on the zeolite particles, their excited states became longer-lived (ca. 100 ns) as compared to the solution counterparts (ca. 13 ns under nitrogen), which also caused a severe retardation to the electron transfer between the electron donors outside the zeolite particles and the $DCA^*_{(NaY)}$ and $CA^*_{(NaY)}$. Iron(II) ions could activate these retarded photoinduced electron transfer reactions. Under the photocatalysis of the NaY/Fe^{2+}/DCA particle, $P(C_6H_5)_3O$ could be generated from $P(C_6H_5)_3$ in aerated CH_3CN. If AgF was added, the major product shifted from $P(C_6H_5)_3O$ to $P(C_6H_5)_3F_2$. Under a similar photolysis condition, $(C_6H_5)_3CF$ was the major derivative of triphenylmethane. These results suggested that $P(C_6H_5)_3{}^+$, $P(C_6H_5)_3{}^{2+}$, and $(C_6H_5)_3C^+$ had been generated. Electron transfer reaction was evidenced to play a key role in the NaY/Fe^{2+}/DCA- and NaY/Fe^{2+}/CA-sensitized photoreactions.

Introduction

Photoinduced electron transfer reactions have been an important impetus to the development of our modern technologies and continue to be the leading topics of current research. A variety of applications, such as chemical degradation,[1] solar energy transduction,[2] molecular photovoltaics,[3] and photosensitization,[4] have been inspired. Many systems have also been studied and shown to be promising in these and many other areas.[5] In a recent attempt to fabricate the nonsilver-based photographic films, we found that many electron deficient sensitizers, like acridinium[6] and 9,10-dicyanoanthracene (DCA),[7] are potential photoanodes in their excited states.

Cyanoanthracenes,[8] such as DCA and 9-cyanoanthracene (CA), have been recognized as effective catalysts for the photooxygenation of organic compounds in aerated solutions.[1,7−9] This application potential is partly merited by the fact that these species in their excited states may compete with inorganic oxidants, like permanganate or peroxydisulfate. Although the charge separation states of DCA and CA are shorter-lived as compared to the triplet excited ruthenium trisbipyridine ($Ru(bpy)_3{}^{2+}$*, ^{3}MLCT),[10] only one way electron transfer from the electron donor to their excited states is permitted. Regarding the DCA- and CA-sensitized photooxygenations, two pathways, electron transfer and energy transfer, are often argued.[11] In the energy transfer pathway, singlet oxygen ($^1O_2$) may be generated. Superoxide anion radical ($O_2{}^{\bullet-}$) can be produced as well, but it is believed to result from the electron transfer route. For the identification of these pathways and the involved reactive oxygen species, substituted butadienes, like *trans*,*trans*-1,4-diphenyl-1,3-butadiene (DPB), are recognized as effective probes.[12] Endoperoxide can derive from the singlet oxygen pathway. On the other hand, monooxygenated products, like benzylaldehydes, are considered as the characteristic products from the superoxide reaction. However, recent studies have pointed out that dioxane and endoperoxide, once thought of as the products characteristic of a singlet oxygen reaction, can also be generated by electron transfer photooxygenation.[13] Regarding the DCA- and CA-sensitized electron transfer reactions, we recently characterized the energetics of the excited DCA and CA using diphenylamine (DPA) and triphenylphosphine ($P(C_6H_5)_3$) as the redox probes. The formal potentials of the excited DCA and CA are confirmed to be located between the formal potentials of $DPA^{+/0}$ and the formal potentials of $P(C_6H_5)_3{}^{+/0}$, which agree well with the results calculated based on the ground state reduction potentials of both DCA and CA and their zero−zero transition energy. In this study, we also prepared the DCA- and CA-exchanged zeolite particles as the heterogeneous catalysts for the photooxygenation of organic compounds. We find that the entrapped DCA* and CA* become longer-lived as compared to the solution counterparts. Besides, the photoinduced electron injection allowed from DPA to $DCA^*_{(solution)}$ and $CA^*_{(solution)}$ is restricted as DCA and CA are adsorbed on the zeolite particles. These results imply that the adsorbed sensitizers are entrapped deep inside the aluminosilicate host. By incorporating iron(II) ions into these modified zeolite particles (denoted NaY/Fe^{2+}/DCA and NaY/Fe^{2+}/CA), the photoinduced electron transfer between the entrapped

* To whom correspondence should be addressed. E-mail: checmw@scc.ntnu.edu.tw.

10.1021/jp021852j CCC: $25.00
Published on Web 01/28/2003

sensitizers and the donors can thus be retrieved. The ^{31}PNMR and ^{19}FNMR analyses show that triphenylphosphine and triphenylmethane can be converted into $P(C_6H_5)_3O$, $P(C_6H_5)_3F_2$, and $(C_6H_5)_3CF$ in aerated CH_3CN under the catalysis of the NaY/Fe^{2+}/DCA particles in the presence of AgF. These results indicate that $P(C_6H_5)_3^+$, $P(C_6H_5)_3^{2+}$, and $(C_6H_5)_3C^+$ have been generated. Electron transfer is evidenced to play a crucial role in the photoreactions sensitized by the NaY/Fe^{2+}/DCA and NaY/Fe^{2+}/CA particles.

Experimental Section

CA and DCA were supplied by TCI. DPA, triphenylphosphine, triphenylmethane, zeolite Y (NaY), and iron(II) sulfate were also purchased from Aldrich.

The DCA- and CA-modified zeolite particles were prepared as follows: 1 g of zeolite Y (NaY) was first suspended in 500 mL of NaCl (1 M) for 6 h. This process was repeated several times to ensure that the ion exchange sites on the zeolite particles were in the Na form. The slurry was thoroughly washed with deionized water until no chloride was detected with silver nitrate. The NaY particles were dried under vacuum and then allowed to soak in the solutions containing DCA and CA (1 mM in CH_3CN), respectively, for 2 days. This was followed by extensive wash with CH_3CN to remove the unreacted sensitizers. The resulting slurries (denoted NaY/DCA and NaY/CA) were then air-dried and stored under nitrogen. The loadings of DCA and CA in the resulting NaY particles were estimated to be less than 0.1 μmol g^{-1} based on the comparison between their emission spectra and the spectra from the solution counterparts. The NaY/DCA and NaY/CA particles were resuspended in aqueous $FeSO_4$ (1 mM) for 12 h. After they were carefully filtered and washed with deionized water, the Fe^{2+}-exchanged NaY/DCA and NaY/CA particles (denoted NaY/Fe^{2+}/DCA and NaY/Fe^{2+}/CA) were air-dried and stored under nitrogen.

Unless otherwise mentioned, the photoelectrochemical experiments were carried out under nitrogen in a one compartment cell using a standard three electrode configuration. A quartz cuvette (10 mm × 10 mm × 50 mm) was used as the electrochemical cell. On one wall of the cuvette, an optical window (5 mm × 5 mm) was opened for photolysis; the rest area was covered with black tapes. A Pt electrode and a silver pseudo-reference electrode were used as the counter and reference electrodes. Both were kept below the optical window to avoid any unnecessary illumination. The formal potentials of redox couples were measured with a homemade glassy carbon electrode (0.28 cm^2). The electrode surface was kept perpendicular to the optical window. Potentials were calibrated against ferrocene ($E°'$: 0.38 V vs SCE in $TBAClO_4/CH_3CN$). Potentiostats (PAR 283, EG&G Princeton Applied Research, and CV-50, Bioanalytical System Inc.) were used to obtain $i-E$ curves and for electrolysis experiments. The electrical signals were recorded and analyzed with a microcomputer. The diffuse−reflectance UV−vis absorption spectra were recorded with a UV−vis spectrophotometer (JASCO model 7850). The steady state emission spectra were recorded with a luminescence spectrometer (Aminco-Bowman series 2) in conjugation with a Hamamatsu R 2949 photomultiplier tube. The diffuse−reflectance emission spectra were measured with the Aminco-Bowman luminescence spectrometer coupled with a Y type optical fiber (Oriel model 77404). A high-pressure mercury lamp (1000 W, Oriel) with a 10 cm long homemade water filter and desired band-pass filters (e.g., 365 and 260 nm, Toptical Scientific) was employed as the light source. The transient emission spectra were recorded with a luminescence spectrometer (OB 920, Edinburgh Instruments Ltd., U.K.) coupled with an nF900 nanosecond flashlamp. In these flash photolysis experiments, all samples (ca. 0.3 g L^{-1}) were prepared and degassed prior to laser experiments. Luminescence decay kinetics were deconvoluted from the instrumental response function to give the single exponential decays. The ^{19}FNMR, ^{31}PNMR, ^{1}HNMR, and ^{13}CNMR were recorded at 400 MHz on a JEOL JNM EX400 spectrometer. Chemical shifts reported in ^{19}FNMR were referenced to $CFCl_3$. $CFBr_3$ was used as the internal standard (7.38 ppm downfield from $CFCl_3$). Phosphoric acid was used as the ^{31}PNMR internal standard.

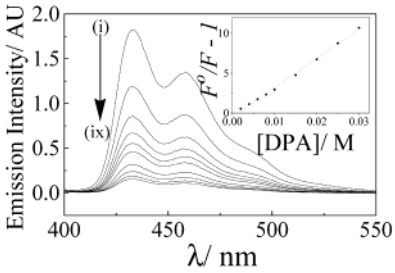

Figure 1. Emission quenching of DCA (1 μM; λ_{ex}, 380 nm; N_2) by DPA at (i) 0, (ii) 2, (iii) 4, (iv) 6, (v) 8, (vi) 10, (vii) 15, (viii) 20, and (ix) 25 mM in CH_3CN. Inset: Stern−Volmer plots between $F/F°$ vs [DPA].

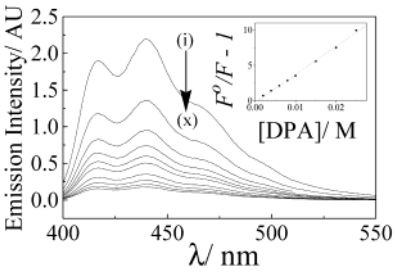

Figure 2. Emission quenching of CA (1 μM; λ_{ex}, 380 nm; N_2) by DPA at (i) 0, (ii) 2, (iii) 4, (iv) 6, (v) 8, (vi) 10, (vii) 15, (viii) 20, (ix) 25, and (x) 30 mM in CH_3CN. Inset: Stern−Volmer plots between $F/F°$ vs [DPA].

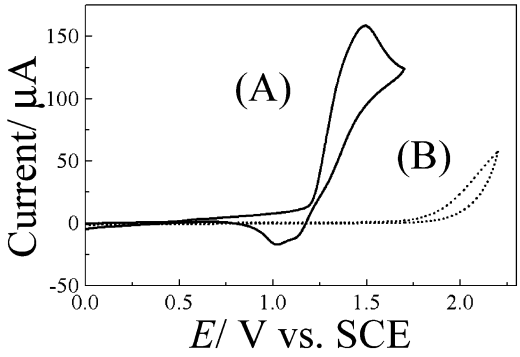

Figure 3. CV curves for 1 mM DPA (A) and 3 mM of $P(C_6H_5)_3$ (B) in $TBAClO_4$ (0.1 M)/CH_3CN. Scan rate: 50 mV s^{-1}.

Results and Discussion

Electron deficient organic compounds are potential photoanodes in their excited states. The representative examples are DCA and CA. It has been reported that two major reaction pathways, energy and electron transfers, are often encountered in the DCA- and CA-sensitized photoreactions.[9] Regarding the DCA- and CA-sensitized electron transfer reactions, experimental results (Figures 1 and 2) indicate that the excited DCA and CA (denoted DCA* and CA*) may photooxidize DPA (E_{pa} ≈ 1.5 V vs SCE; Figure 3A). This possibility is reflected in a decrease in the emission intensities of DCA and CA during the

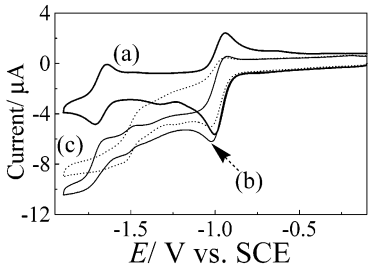

Figure 4. CV curves for 0.1 mM DCA in $TBAClO_4$ (0.1 M)/CH_3CN under the conditions (a) dark, (b) under illumination (365 nm), and (c) illuminated and further added with 1 mM DPA. Scan rate: 50 mV s^{-1}.

addition of DPA. A linear relationship is observed between the reciprocal of the emission intensity (F^{-1}) and the activity of DPA (insets in Figures 1 and 2):

$$F^\circ/F = 1 + \tau^\circ k_Q[\mathrm{DPA}] \quad (1)$$

Here, F° and F are the emission intensities of DCA or CA in the absence and in the presence of a quencher, and τ° is the lifetime of the excited sensitizer in the absence of a quencher. The lifetimes (τ°) of DCA* (λ_{em}, 430 nm) and CA* (λ_{em}, 440 nm) are measured as 12.5 and 12.8 ns, respectively, based on the time-correlated single photon counting techniques. According to these data and the linear plots displayed in Figures 1 and 2, the quenching constants (k_Q) for DCA* and CA* are calculated to be about 4×10^4 equiv^{-1} s^{-1}. The estimation of k_Q based on other emission bands of DCA and CA gave similar results. We hypothesize that these quenching phenomena are caused by the following electron transfer reaction:

$$\mathrm{Sens}^* + \mathrm{DPA} \rightarrow \mathrm{Sens}^- + \mathrm{DPA}^+ \quad (2)$$

Here, Sens designates DCA or CA. Electrochemical characterizations support this postulate. DCA possesses two well-defined redox waves near −1.0 and −1.7 V vs SCE in CH_3CN. The CV curves are shown in Figure 4, trace a). The peak separation in each wave approximates 60 mV. Reversible one electron transfer reactions are considered to participate in both of the waves. We attribute them to $DCA^{0/-}$ and $DCA^{-/2-}$, respectively. Regarding the CV waves of $DCA^{0/-/2-}$, it has been reported that they might be observed at more negative potentials in other media.[14] Despite this discrepancy, closer examinations on these waves show that the second wave in trace a ($DCA^{-/2-}$) is less significant in current than the first one ($DCA^{0/-}$). The trace amount of proton or oxygen dissolved in the solution is considered as the main cause of this phenomenon. According to the formal potentials of $DCA^{0/-}$, $DCA^{-/2-}$, H^+ (E°, −0.244 V vs SCE), and O_2 (E°, 1.0 V vs SCE), proton and oxygen are capable of oxidizing DCA^- and DCA^{2-} and causing a decrease in [DCA^-] and [DCA^{2-}]. The shape of the second wave, or more precisely, the currents of $DCA^{-/2-}$, are thus smaller than expected. Likely resulting from a similar effect, the anodic currents in both CV waves are less significant than the counterpart cathodic currents. Apart from these discrepancies, the cathodic waves of DCA are found sensitive to light illumination. When DCA is illuminated (white light with a 365 nm band-pass filter), the currents of $DCA^{0/-/2-}$ (especially, $DCA^{-/2-}$) are raised greatly (Figure 4, trace b) as compared to the currents recorded in the dark (trace a). The enhancement in current indicates that a greater amount of electrons flow from the electrode to the illuminated DCA, presumably DCA*:

$$\mathrm{DCA}^* + e^- \rightarrow \mathrm{DCA}^-,\ E^{\circ\prime} = 1.9\ \mathrm{V\ vs\ SCE} \quad (3)$$

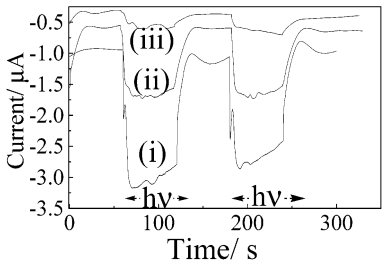

Figure 5. Chronoamperograms recorded for 0.1 mM CA under illumination (365 nm) with the addition of DPA at (i) 0, (ii) 0.1, and (iii) 1 mM. E_{appl}: −1.55 V vs SCE.

While, in the presence of DPA, the observed photocurrent is suppressed significantly (trace c). DPA shows a similar reductive quenching effect on $CA^{*/-}$ (Figure 5). As the electrode potential is set at −1.55 V vs SCE, namely, 150 mV more negative than the formal potential of $CA^{0/-}$ ($E^{\circ\prime} \approx -1.4$ V in CH_3CN), the current associated with $CA^{0/-}$ is enhanced greatly upon exposing the system to light (white light with a 365 nm band-pass filter). However, the amplitude of the photocurrent decreases systematically with the addition of DPA. Reaction 2 is thus believed to play a crucial role in these electrochemical phenomena.

Reaction 2 is thermodynamically favorable from an energetic point of view. The free energy changes (ΔG) are calculated to be −0.4 and −0.1 eV, respectively, for DCA* and CA*. Here, the calculation of ΔG was based on the formal potential of $DPA^{+/0}$ (ca. 1.5 V vs SCE) estimated from the CV curves displayed in Figure 3A and the formal potentials of $DCA^{*/-}$ and $CA^{*/-}$ determined from the associated ground state reduction potentials and zero−zero band transition (λ_{0-0}, 425 and 410 nm, respectively, estimated from the excitation and emission spectra measured in CH_3CN). The energy gaps between the excited and the ground states of DCA and CA (denoted $E_{g,DCA}{}^{0/*}$ and $E_{g,CA}{}^{0/*}$) are calculated to be 2.9 and 3.0 eV, respectively. The formal potentials of $DCA^{*/-}$ and $CA^{*/-}$ (denoted $E^{\circ\prime}{}_{DCA}{}^{*/-}$ and $E^{\circ\prime}{}_{CA}{}^{*/-}$) are thus estimated roughly to be 1.9 and 1.6 V vs SCE. The negative ΔG indicates that DCA* and CA* are powerful oxidants. Regarding the electrochemical phenomena recorded in Figures 4 and 5, we consider that they are less likely to be occasioned by the collisional energy transfer, like:

$$\mathrm{Sens}^* + \mathrm{DPA} \rightarrow \mathrm{Sens} + \mathrm{DPA} + \mathrm{heat} \quad (4)$$

If it were the case, DCA* and CA* would be deactivated by DPA. The concentrations of the ground state DCA and CA in the depletion region near the electrode surface would be increased instead. Further enhancement in currents via an EC′-like mechanism would be observed as a result. For photoinduced electron transfer systems, Weller has suggested that k_Q can be regarded as a function of the overall free energy difference (ΔG) between reactant and product states and the free energy of the transition state (ΔG^*) in the following hypothetic elementary steps:[15]

$$\mathrm{Sens}^* + \mathrm{D} \rightarrow [\mathrm{Sens}^*\mathrm{D}],\ \Delta G^* \quad (5)$$

$$[\mathrm{Sens}^*\mathrm{D}] \rightarrow \mathrm{Sens}^- + \mathrm{D}^+ \quad (6)$$

$$k_Q \approx 2 \times 10^{10}\ \mathrm{equiv}^{-1}\,\mathrm{s}^{-1}/\{1 + 0.25[\exp(\Delta G^*/RT) + \exp(\Delta G/RT)]\} \quad (7)$$

Here, D is the electron donor. If $\Delta G < -0.44$ eV/mol, the magnitude of fluorescence quenching rate constant will reach the diffusion-controlled limit ($k_Q = 2 \times 10^{10}$ equiv^{-1} s^{-1}). Correlations of the k_Q resolved from our system with eq 7

SCHEME 1: Energetic Diagrams for the Electron Transfer between DPA and $P(C_6H_5)_3$ and DCA* and CA*

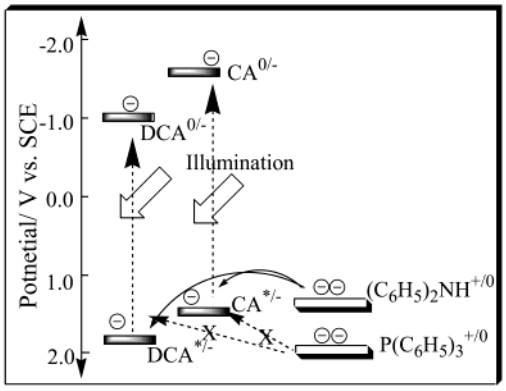

suggest that our k_Q is less significant than expected. By plugging k_Q and ΔG into eq 7, we calculated the ΔG^* for the reactions between DCA* and CA* and DPA to be 0.4 eV. The positive ΔG^* suggests that transition states, like [DCA*DPA] and [CA*DPA], may exist in these photoinduced electron transfer reactions. Probably because of the existence of activation barriers in these systems, the observed k_Q values are smaller than those expected even though the overall reactions are exothermal.

Electron transfer probing of $DCA^{*/-}$ and $CA^{*/-}$ was also carried out with triphenylphosphine ($P(C_6H_5)_3$). Control experiments show that $P(C_6H_5)_3$ does not quench DCA* or CA* as DPA does. Cyclic voltammetry reveals that the oxidation of triphenylphosphine is a sluggish, irreversible process (Figure 3B). The onset potential is ca. 1.8 V vs SCE. Provided that the formal potential of $P(C_6H_5)_3^{+/0}$ is equivalent to its anodic half-peak potential ($E_{p/2,a}$), the formal potential of $P(C_6H_5)_3^{+/0}$ is estimated to be around 2 V vs SCE, more positive than 1.8 V. This result indicates that the formal potential of $P(C_6H_5)_3^{+/0}$ is very close to or more positive than $E^{\circ\prime}_{DCA^{*/-}}$ and $E^{\circ\prime}_{CA^{*/-}}$. The following electron transfer reaction is thus considered unfavorable:

$$\text{Sens}^* + P(C_6H_5)_3 \rightarrow \text{Sens}^- + P(C_6H_5)_3^+,\ \Delta G > 0 \quad (8)$$

We summarize the energetics of the species involved in reactions 2 and 8 in Scheme 1 for comparison. Although the ground state $P(C_6H_5)_3$ is not powerful in reducing DCA* or CA*, its excited state ($P(C_6H_5)_3$*) is theoretically able to quench DCA* and CA*, namely,

$$\text{Sens}^* + P(C_6H_5)_3^* \rightarrow \text{Sens}^- + P(C_6H_5)_3^+ \quad (9)$$

For this possibility, we calculate the associated ΔG to be -4.7 eV for DCA* and -4.1 eV for CA*. Here, the formal potential of $P(C_6H_5)_3^{+/*}$ is estimated to be -2.7 V vs SCE based on the excitation energy for $P(C_6H_5)_3^{0/*}$ and the formal potential of $P(C_6H_5)_3^{+/0}$ (2.0 V vs SCE, presumably). $P(C_6H_5)_3$ is fluorescence inactive. The energy gap between its first excited state and its ground state is approximated to be 4.7 eV based on the absorption peak recorded at 260 nm ($\lambda_{ab,max}$). Experimental results displayed in Figure 6 support our hypothesis, showing that when $P(C_6H_5)_3$ and DCA and CA are photoexcited with 260 nm light, $P(C_6H_5)_3$* can quench DCA* (Figure 6A) and CA* (B). Therefore, the formal potentials of $DCA^{*/-}$ and $CA^{*/-}$ are believed to be located between the formal potentials of $DPA^{+/0}$ and the formal potentials of $P(C_6H_5)_3^{0/+}$, which are in a good agreement with the predicted values.

DCA* and CA* may induce photooxidation of electron donors, but they are less suitable to function as photocathodes.

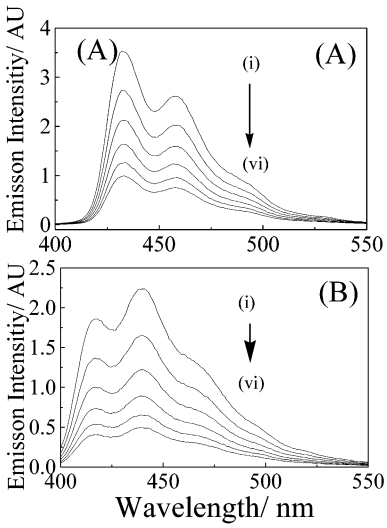

Figure 6. Emission quenching (λ_{ex}, 260 nm) of DCA (A) and CA (B) by $P(C_6H_5)_3$ at (i) 0, (ii) 20, (iii) 40, (iv) 60, (v) 80, and (vi) 100 mM.

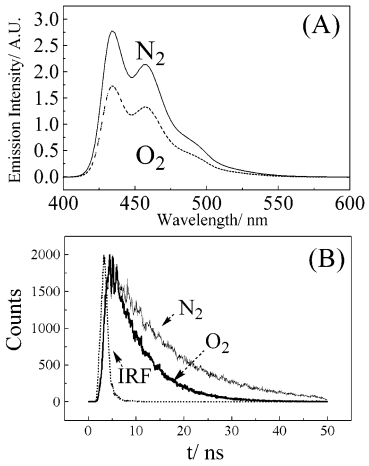

Figure 7. Oxygen effects on the emission of DCA (A) and the lifetime of DCA* (B) in CH_3CN. IRF: instrumental response function.

This hypothesis is supported by the facts that H_2O_2 and $S_2O_8^{2-}$ do not exhibit any quenching effects on DCA*. Nevertheless, oxygen is found as an effective quencher. Figure 7 shows that the emission intensity of DCA (1 μM in CH_3CN, A) and the lifetime of DCA* (B) decrease significantly as oxygen is introduced into the system. Oxygen also shows a similar quenching effect on CA*, causing the lifetime of CA* (λ_{em}, 440 nm; λ_{ex}, 380 nm) to decrease from 12.8 (under N_2) to 6.6 ns. Theoretically, hydrogen peroxide and peroxydisulfate ion are more powerful in oxidation than oxygen according to their standard reduction potentials:

$$O_2 + 2e^- + 2H^+ \rightarrow H_2O_2,\ E^\circ = 0.68 \text{ V vs NHE} \quad (10)$$

$$H_2O_2 + 2e^- + 2H^+ \rightarrow 2H_2O,\ E^\circ = 1.78 \text{ V vs NHE} \quad (11)$$

The insignificant effects of H_2O_2 and $S_2O_8^{2-}$ on DCA* and CA* indicate that the photoinduced electron injection from electron deficient sensitizers to electron acceptors is not favorable. This conclusion, in turn, highlights that the quenching effect of oxygen is through a collisional energy transfer:

$$\text{Sens} + h\nu \rightarrow {}^1\text{Sens}^* \quad (12)$$

$${}^1\text{Sens}^* + {}^3O_2 \rightarrow {}^3\text{Sens}^* + {}^1O_2 \quad (13)$$

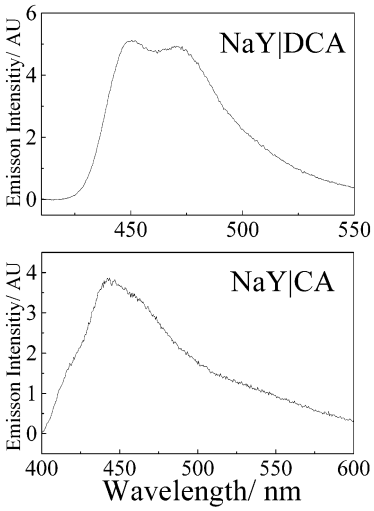

Figure 8. Typical diffuse−reflectance emission spectra for the NaY/DCA and NaY/CA particles (λ_{ex} 380 nm).

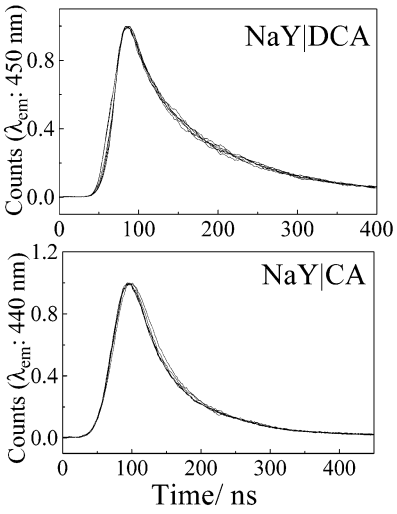

Figure 9. Transient emission spectra of DCA*$_{(NaY)}$ and CA*$_{(NaY)}$ (λ_{ex} 365 nm) in the presence of DPA. [DPA]: 0−10 mM in CH_3CN.

Singlet oxygen is a reactive species. Its formation and participation is theoretically able to assist the oxygenation of organic compounds. For the oxygenation of DPA and $P(C_6H_5)_3$ in aerated solutions, we prepared the DCA- and CA-exchanged zeolite (NaY) particles (denoted NaY/DCA and NaY/CA) as the heterogeneous catalysts. We expect that the use of zeolite may prevent the undesired back reactions from occurring. Diffuse−reflectance emission spectroscopic analyses confirm that DCA and CA can be exchanged into the NaY particles. The typical spectra are shown in Figure 8. As compared to the spectra shown in Figures 1 and 2, the emission bands revealed from DCA$_{(NaY)}$ (A) and CA$_{(NaY)}$ (B) shift to longer wavelengths. These bathochromic shifts suggest that the DCA*$_{(NaY)}$ and CA*$_{(NaY)}$ species are stabilized by the zeolite host. The energy gap between the ground and the excited states of the adsorbed sensitizer is thus reduced, resulting in bathochromic shifts. Transient emission spectral measurements support this hypothesis. Figure 9 shows that the lifetimes of DCA*$_{(NaY)}$ and CA*$_{(NaY)}$ become 125 and 82 ns, respectively, which are much longer than the solution counterparts (ca. 13 ns). In addition, the DCA* $_{(NaY)}$ and CA* $_{(NaY)}$ species show indifferent responses to the addition of DPA, reflected in the insignificant change in the lifetimes of the excited sensitizers during the addition of

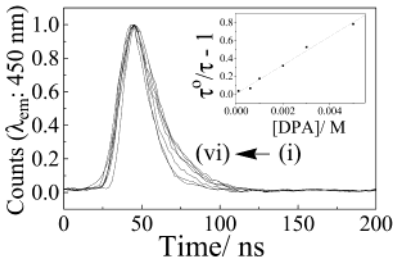

Figure 10. Transient emission spectra recorded for NaY/Fe^{2+}/DCA (λ_{ex}, 365 nm) in the presence of DPA. [DPA]: (i) 0, (ii) 0.1, (iii) 0.5, (iv) 1.5, (v) 2.0, and (vi) 4.0 mM in CH_3CN. Inset: Plots of $\tau°/\tau$ vs [DPA].

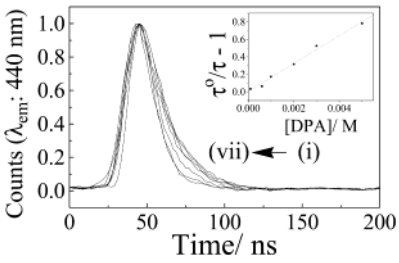

Figure 11. Transient emission spectra measured for NaY/Fe^{2+}/CA (λ_{ex}, 365 nm) in the presence of DPA. [DPA]: (i) 0, (ii) 0.1, (iii) 0.6, (iv) 1.0, (v) 2.0, (vi) 3.0, and (vii) 5.0 mM in CH_3CN. Inset: Plots of $\tau°/\tau$ vs [DPA].

quencher. These behaviors seem not found in the ZSM-5 system.[9] These results strongly suggest that the DCA$_{(NaY)}$ and CA$_{(NaY)}$ species are confined within the zeolite host. This effect minimizes the probability for vibrational relaxation. It also restricts the electron transfer from electron donors to the entrapped sensitizers. In improving the communication between the entrapped sensitizers and the DPA, we find it useful using Fe^{2+} ions as the mediator. After incorporating Fe^{2+} ions in the NaY/DCA and NaY/CA particles (denoted NaY/Fe^{2+}/DCA and NaY/Fe^{2+}/CA), experimental results (Figures 10 and 11) show that the DCA* $_{(NaY)}$ and CA* $_{(NaY)}$ species become shorter-lived ($\tau \approx 17$ ns). This action, in addition, retrieves the sensitivity of DCA$_{(NaY)}$* and CA$_{(NaY)}$* to DPA, leading to a decrease in the lifetimes (τ) of DCA* and CA* with an increase in [DPA]:

$$\tau°/\tau = 1 + \tau° \, k_Q'[\mathrm{DPA}] \qquad (14)$$

The apparent Stern−Volmer quenching constants, k_Q', are calculated to be 1×10^{10} M^{-1} s^{-1} for NaY/Fe^{2+}/DCA and NaY/Fe^{2+}/CA (insets in Figures 10 and 11). Regarding the effect of Fe(II) ions, we have recently reported that the iron species contained in iron-containing clay minerals are effective mediators and they can mediate electron transfer reactions taking place on the clay surface.[16] Accordingly, we propose a reaction mechanism as shown in Scheme 2 and eqs 15 and 16, in which $Fe^{3+/2+}$ bridges the communication between the entrapped sensitizers and the DPA.

$$\mathrm{Sens}^*_{(NaY)} + \mathrm{Fe}^{2+}{}_{(NaY)} \rightarrow \mathrm{Sens}^-{}_{(NaY)} + \mathrm{Fe}^{3+}{}_{(NaY)} \qquad (15)$$

$$\mathrm{Fe}^{3+}{}_{(NaY)} + \mathrm{DPA}_{(solution)} \rightarrow \mathrm{Fe}^{2+}{}_{(NaY)} + \mathrm{DPA}^+{}_{(solution)} \qquad (16)$$

To complete the reaction cycle, oxygen, Ag^+, and many other oxidants of which the formal potentials are more positive than $E°'_{DCA}{}^{0/-}$ are qualified electron acceptors. In the experiments using oxygen as the electron acceptor (Supporting Information 1A), about 31% of $P(C_6H_5)_3$ can be converted into $(C_6H_5)_3PO$

SCHEME 2: Schematic Illustrations for the Photoinduced Electron Transfer Taking Place on the Sensitizer-Modified Zeolite Particles[a]

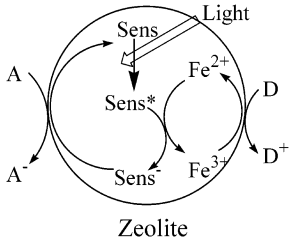

$A = O_2, Ag^+$

$D = DPA, P(C_6H_5)_3$

[a] Sens: DCA or CA.

in aerated CH_3CN under the catalysis of the NaY/Fe^{2+}/DCA particle:

$$P(C_6H_5)_3 \xrightarrow[NaY/Fe^{2+}/DCA]{O_2,\ h\nu} (C_6H_5)_3PO \qquad (17)$$

Here, the yield was analyzed by ^{31}PNMR. The photolysis was provided by a 1000 W Xe lamp with a 260 nm band-pass filter; the photolysis proceeded for 30 s. Control experiments show that most $P(C_6H_5)_3$ remains intact if DCA is excluded from the zeolite particle (Supporting Information 1B). This result suggests that the excited oxygen does not cause significant oxidation of $P(C_6H_5)_3$. In these experiments, no other products were found according to ^{13}CNMR and ^{1}HNMR. Regarding the DCA-sensitized photooxygenations, literatures suggest that singlet oxygen ($^1O_2$) may be involved.[9] To identify the reactive oxygen species involved in our system, we had used DPB as the probe of $^1O_2$. Product analyses showed that the amount of endoperoxide was not very significant, whereas monooxygenated products, like benzylaldehyde, were found as the major products. These results imply that the photooxygenation reaction in our system is mainly caused by superoxide radical anion through an electron transfer route. $^1O_2$ appears less compatible with $O_2^{\bullet-}$ in amount or reaction rate in this case. Supports for this postulate come from the experiments by adding AgF (2 equiv to $P(C_6H_5)_3$) intentionally with oxygen as electron acceptors. The ^{19}FNMR analysis (Supporting Inforamtion 2A) indicates that a variety of fluorinated products are formed. $(C_6H_5)_3PF_2$ is identified as the major product (40.0 ppm (d) upfield from $CFCl_3$; J_{PF}, 663 Hz; yield, 14%). Yields reported here are from integration of NMR spectra and do not represent isolated yields. C_6F_6 (δ, −164.9 ppm) was added as internal standard for yield estimation. $(C_6H_5)_3PO$ is also formed, but the yield appears less significant as compared to $(C_6H_5)_3PF_2$ according to ^{31}PNMR (Supporting Information 2B). Silver ion is unable to oxidize $P(C_6H_5)_3$. $(C_6H_5)_3PF_2$ apparently derives from $(C_6H_5)_3P^+$ and $(C_6H_5)_3P^{2+}$ via the following reactions:

$$DCA^*_{(NaY)} + Fe^{2+}_{(NaY)} \rightarrow DCA^-_{(NaY)} + Fe^{3+}_{(NaY)} \qquad (18)$$

$$Fe^{3+}_{(NaY)} + (C_6H_5)_3P^*_{(solution)} \rightarrow (C_6H_5)_3P^+_{(solution)} + Fe^{2+}_{(NaY)} \qquad (19)$$

$$Fe^{3+}_{(NaY)} + (C_6H_5)_3P^+_{(solution)} \rightarrow (C_6H_5)_3P^{2+}_{(solution)} + Fe^{2+}_{(NaY)} \qquad (20)$$

$$(C_6H_5)_3P^{2+}_{(solution)} + 2F^-_{(solution)} \rightarrow (C_6H_5)_3PF_{2(solution)} \qquad (21)$$

$$DCA^-_{(NaY)} + Ag^+_{(solution)} \rightarrow DCA_{(NaY)} + Ag_{(NaY)} \qquad (22)$$

Theoretically, silver ion can be oxidized by $DCA^*_{(NaY)}$ into higher valence species, like Ag^{2+}, and assist the photofluorination of $(C_6H_5)_3P$. Apart from these possibilities, electron transfer is evidenced as the dominating process in the overall reaction. Under a similar photolysis condition, triphenylmethane ($(C_6H_5)_3CH$) could be converted into $(C_6H_5)_3CF$ (−126.5 ppm (s) vs $CFCl_3$). According to ^{19}FNMR and ^{1}HNMR, the selectivity was very high although the yield was low, about 2%. No other products were found. The formation of $(C_6H_5)_3CF$, in addition, supports that electron transfer reaction plays a key role in the NaY/Fe^{2+}/DCA- and NaY/Fe^{2+}/CA-sensitized photoreactions.

Acknowledgment. The authors thank the National Science Council, Republic of China (NSC 90-2113-M-003-019) and National Taiwan Normal University (ORD-90-2) for financial support.

Supporting Information Available: Spectra using oxygen as the electron acceptor and ^{19}FNMR spectra. This material is available free of charge via the Internet at http://pubs.acs.org.

References and Notes

(1) Shiraishi, Y.; Taki, Y.; Hirai, T.; Komasawa, I. *J. Chem. Soc. Chem. Commun*. **1998**, 2601.

(2) Gust, D.; Moore, T. A.; Moore, A. L. *Acc. Chem. Res*. **2001**, *34*, 40.

(3) Hagfeldt, A.; Grätzel, M. *Acc. Chem. Res*. **2000**, *33*, 269.

(4) Ikeda, H.; Minegishi, T.; Abe, H.; Konno, A.; Goodman, J. L.; Miyashi, T. *J. Am. Chem. Soc*. **1998**, *120*, 87.

(5) (a) Wilson, R.; Akhavan-Tafti, H.; DeSilva, R.; Schaap, A. P. *Anal. Chem*. **2001**, *73*, 763. (b) Grant, C. D.; Schwartzberg, A. M.; Smestad, G. P.; Kowalik, J.; Tolbert, L. M.; Zhang, J. Z. *J. Electroanal. Chem*. **2002**, *522*, 40. (c) Eugster, N.; Fermín, D. J.; Girault, H. H. *J. Phys. Chem. B* **2002**, *106*, 3428. (d) Rolison, D. R.; Bessel, C. A. *Acc. Chem. Res*. **2000**, *33*, 737.

(6) Liou, Y.-W.; Wang, C. M. *J. Chem. Soc. Chem. Commun*. **2000**, 27.

(7) (a) Chang, J.-J.; Wang, C. H.; Wang, C. M. *International Symposium on Design of Electron Transfer Systems for Green Organic Synthesis and New Intelligent Materials (IS-DET Okayama)* **2002**, 7. (b) Liou, Y.-W.; Wang, C. M. *J. Chin. Chem. Soc*. **2002**, *49*, 51.

(8) Kavarnos, G. J.; Turro, N. J. *Chem. Rev*. **1986**, *86*, 400.

(9) Tung, C. H.; Wang, H.; Ying, Y. M. *J. Am. Chem. Soc*. **1998**, *120*, 5179.

(10) (a) Balzani, V.; Juris, A. *Coord. Chem. Rev*. **2001**, *211*, 97. (b) Demas, J. N.; DeGraff, B. A. *Anal. Chem*. **1991**, *63*, 829 A.

(11) (a) Foote, C. S. *Photochem. Photobiol*. **1991**, *54*, 659. (b) Mataga, N.; Mitiga, M.; Nishimura, T. *J. Mol. Struct*. **1978**, *47*, 199.

(12) (a) Kanner, R. C.; Foote, C. S. *J. Am. Chem. Soc*. **1992**, *114*, 678. (b) Gerson, F.; Lopez, J.; Krebs, A.; Rugner, W. *Angew. Chem., Int. Ed. Engl*. **1981**, *20*, 95.

(13) Kabe, Y.; Takata, Y.; Ueno, K.; Ando, W. *J. Am. Chem. Soc*. **1984**, *106*, 8174.

(14) Ishiguro, K.; Ikeda, M.; Sawaki, Y. *J. Org. Chem*. **1992**, *57*, 3057.

(15) Rehm, D.; Weller, A. *Isr. J. Chem*. **1970**, *8*, 259.

(16) Teng, Y.-W.; Chang, I.-J.; Wang, C. M. *J. Phys. Chem. B* **1997**, *101*, 10386.